**Wave: Jurnal Ilmiah Teknologi Maritim** **Vol. 19 No. 02, December 2025: page: 107-117**
**(Journal of Maritime Technology)** p - ISSN: 1978-886X
e - ISSN: 2614-641X

# An Integrated Solver-CFD Framework for the Optimization and Open-Water Performance Evaluation of Wageningen B-Series Marine Propellers

**Muhammad Ali Reza[1], Lilik Khoiriyah[2,*], Muhammad Fiky Izzulhaq[1], Intan Rahmahwati[1], Vena Rizky Pusparani[1] and Chezta Ahmad Muzakky[1]**

[1]Department of Marine Engineering, Politeknik Perkapalan Negeri Surabaya, Surabaya, Indonesia
[2]Department of Naval Architecture, Politeknik Perkapalan Negeri Surabaya, Surabaya, Indonesia

**Article Info**

***Article history:***
Received October 31, 2025
Revised December 19, 2025
Accepted December 31, 2025

***Keywords:***
Wageningen B-series Propeller
Computational Fluid Dynamics (CFD)
Solver
Propeller Optimization
Open Water Performance

**ABSTRACT**

This study investigates the optimization of Wageningen B-series marine propellers using a CFD-based approach combined with numerical solver techniques to improve hydrodynamic performance under operational constraints. Key design parameters, including blade number, diameter, pitch ratio, and expanded area ratio, were optimized while satisfying thrust, cavitation, and structural limits. Propeller performance was evaluated in terms of thrust coefficient (KT), torque coefficient (KQ), and open water efficiency (η), with and without the application of Propeller Boss Cap Fins (PBCF). The optimized configuration consists of a three-bladed propeller, achieving a maximum efficiency of 0.51347 while meeting all imposed constraints. Results show that the inclusion of PBCF reduces KT, KQ, and η at low to moderate advance coefficients, but yields efficiency improvements at higher advance coefficients, particularly at J = 0.8. The findings demonstrate that CFD-based constrained optimization provides an effective alternative to conventional chart-based propeller design methods and highlights the importance of matching propeller modifications to specific operating conditions.



***Corresponding Author:***
Lilik Khoiriyah
Department of Naval Architecture
Politeknik Perkapalan Negeri Surabaya
Surabaya, Indonesia
Email: lilikkhoiriyah@ppns.ac.id

## INTRODUCTION

The design of ship propulsion systems is a critical factor influencing vessel performance, energy efficiency, and operational reliability (Gaggero, 2025; Sandjaja et al., 2023). In fixed-pitch propeller applications, particularly for Wageningen B-series propellers, designers must balance hydrodynamic performance indicators

such as thrust coefficient (KT), torque coefficient (KQ), and open water efficiency (η) with constraints related to cavitation, structural strength, propeller diameter, pitch ratio, and operational requirements (He et al., 2024;Ouyang et al., 2025;Kiss-Nagy et al., 2024).

Among these parameters, the selection of blade number and associated geometric characteristics remains a central challenge due to its strong influence on efficiency, cavitation susceptibility, and mechanical reliability (Abar and Utama, 2019). Conventional propeller design methods based on Wageningen B-series charts are still widely applied because of their simplicity and standardization. However, these chart-based approaches rely heavily on manual interpretation, introducing subjectivity and potential inconsistencies in estimating KT, KQ, and η (Mizzi et al., 2017). In addition, the fixed nature of series propeller diagrams limits the ability to systematically evaluate trade-offs between thrust, efficiency, and cavitation over a wide range of operating conditions. Such limitations reduce their robustness in addressing current demands for improved energy efficiency and compliance with increasingly stringent environmental regulations (Sandjaja et al., 2023).

To overcome these constraints, recent studies have increasingly incorporated Computational Fluid Dynamics (CFD) and numerical optimization techniques. CFD provides high-fidelity insight into propeller flow physics, while optimization methods enable structured exploration of design parameters such as blade number, expanded area ratio, and pitch ratio (Gypa et al., 2023; Guan et al., 2022; Trimulyono et al., 2022). However, in many existing studies, optimization is either performed heuristically or relies on metaheuristic algorithms that do not explicitly enforce design constraints within a deterministic solution process. Moreover, CFD is often used as a post-analysis tool rather than being directly integrated into a solver-driven optimization loop.

In parallel, propeller performance enhancement devices such as Propeller Boss Cap Fins (PBCF) have been investigated in several studies, generally reporting potential efficiency gains. Nevertheless, these assessments are frequently conducted independently of the baseline propeller optimization process and are rarely embedded within a constrained numerical framework that accounts for blade number selection, cavitation limits, and thrust requirements simultaneously. As a result, the combined influence of solver-based optimization, blade number selection, and PBCF performance across varying advance coefficients remains insufficiently addressed.

Therefore, a clear research gap remains in the use of solver-based constrained optimization that is tightly integrated with CFD simulations to systematically identify the optimal blade number and geometry of Wageningen B-series propellers under realistic hydrodynamic, cavitation, and structural constraints. This study positions the numerical solver as the main optimization engine, in which objective functions and constraints are explicitly defined and solved, while CFD provides validated hydrodynamic responses within the optimization loop. This solver-assisted framework enables objective, repeatable, and constraint-consistent optimization of standard B-series propellers and allows simultaneous evaluation of the hydrodynamic effects of PBCF over a range of advance coefficients. The integrated approach improves design robustness and helps identify operating conditions where propeller

Vol. 19 No. 02, December 2025: page: 107-117
p - ISSN: 1978-886X
e - ISSN: 2614-641X

modifications yield measurable efficiency gains, supporting more efficient and regulation-compliant propulsion system design (Ristea et al., 2025).

## METHOD

This study adopts a solver-assisted optimization framework integrated with Computational Fluid Dynamics (CFD) to determine the optimal configuration of a Wageningen B-Series propeller, comprising four main stages: (1) formulation of the objective function and optimization constraints based on B-Series characteristics, cavitation criteria, material strength limits, and the required ship thrust; (2) numerical optimization using a deterministic solver; (3) evaluation of hydrodynamic performance through CFD simulations under open-water conditions; and (4) grid-independence testing and validation of the results against reference data of the Wageningen B-Series. This framework ensures physical consistency, result reproducibility, and numerical accuracy throughout the propeller design process.

First, the ship's operational data are specified as fixed input parameters, including the total ship resistance Rt = 337.257 N, engine power P = 5220 kW, draft T = 5,066 m, and service speed Vs = 13 knots (6,6872 m s-1). Based on these parameters, the required thrust Treq and the advance coefficient J are calculated using standard propulsion equations. In addition to these primary parameters, the design adjustment also incorporates supporting data as recommended in the Wageningen B-Series literature, including the maximum allowable propeller diameter, the minimum advance coefficient Jmin and the material properties of the propeller blades. Nickel Aluminium Bronze is adopted as the reference material, and its allowable stress is used as the structural strength limit in the optimization process.

The hydrodynamic characteristics of the propeller are modeled using empirical data from the Wageningen B-Series. The thrust coefficient KT and torque coefficient KQ are approximated using fifth-order polynomial expressions (n=5) derived from the B-Series coefficient tables for each combination of blade number Z, pitch-to-diameter ratio P/D, and expanded blade area ratio Ae/A0. These coefficients are the used to calculate the propeller thrust, torque, and open-water efficiency η, which are subsequently incorporated into the optimization objective function.

The optimization problem is formulated as a constrained nonlinear optimization, with the objective of maximizing open-water efficiency (η):

$$\max \eta = \frac{J K_T}{2 \pi K_Q} \quad (1)$$

subject to the following constraints:

Thrust constraint :

$$T_{CFD} \geq T_{req} \quad (2)$$

Advance coefficient constraint :

$$J_{min} \leq J \leq J_{max} \quad (3)$$

Geometrical constraints:

$$D \geq D_{max} \quad (4)$$

$$\left(\frac{P}{D}\right)_{min} \leq \frac{P}{D} \leq \left(\frac{P}{D}\right)_{max} \quad (5)$$

$$(A_E/A_0)_{min} \leq A_E/A_0 \leq A_E/A_{0_{max}} \quad (6)$$

Cavitation constraint:

$$\tau_c \geq \tau_{c\,limit} \quad (7)$$

where $\tau_c$ represents the local cavitation, index derived from blade loading and pressure distribution.

Material strength constraint:

$$\frac{t_{min}}{D} \geq \left(\frac{t}{D}\right)_{req} \quad (8)$$

where $t_{min}$ is the minimum blade thickness required based on Nickel Aluminium Bronze allowable stress.

For each candidate blade number (Z=3-7), and the thrust coefficient KT and torque coefficient KQ are calculated, including Reynolds number corrections when Rn > 2 x 106. The iterative procedure is continued until all constraints are satisfied and the propeller efficiency reaches a global maximum within the defined design space.

The optimization process for marine propeller selection in solver employs several key constraints as solver parameters, such as ensuring that blade thickness remains below the cavitation limit, the advance coefficient stays above its minimum value, and the pitch-to-diameter ratio does not exceed the maximum allowed. Additionally, the propeller's efficiency must not surpass unity and must be greater than zero, while the diameter must not exceed the specified maximum. Selected values for pitch-to-diameter ratio, advance coefficient, and expanded area ratio must fall within their respective minimum and maximum limits.

The ratio of blade thickness to diameter must be controlled according to both the propeller quantity and material properties. These constraints ensure that the final selected propeller provides safe, effective, and structurally reliable operation under the defined design conditions.

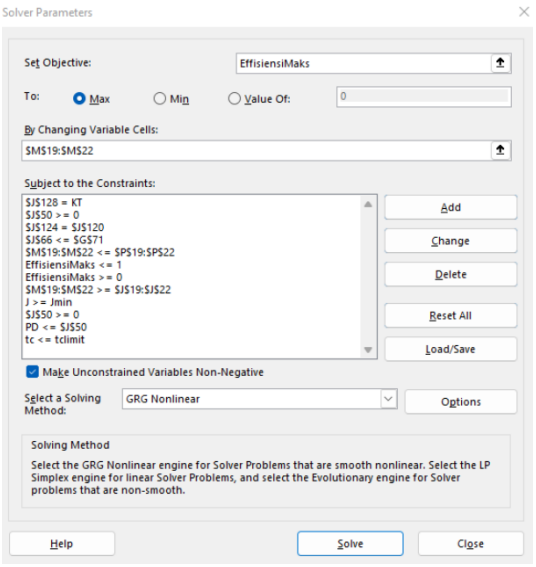


Figure 1. Solver Constraint Settings

Based on iterative results comparing propeller blades with 3, 4, 5, 6, and 7 blades, the optimal iteration result indicated that the propeller with 3 blades is the most effective. The selection parameters for the propeller blades were based on satisfying the condition τc < τc limit as a cavitation limit, where τc is the critical shear stress or cavitation parameter and τc limit is set as boundary value for design and analysis to prevent cavitation inception. [t_min/D]x 0.7 R < tmax/D as a material constraint, where tmin is the minimum thickness refers to the smallest blade thickness at a specific point along the propeller blade radius, D is the propeller diameter is defined as the maximum straight-line distance between two opposing blade tips passing through the center of the propeller and R is the propeller radius. And last parameter is Tcal < 0.001 as a thrust constraint, where tcal is the propeller thrust value obtained from analytical calculations or numerical simulations of the propeller design.

**Wave: Jurnal Ilmiah Teknologi Maritim**
**(Journal of Maritime Technology)**
**Vol. 19 No. 02, December 2025: page: 107-117**
p - ISSN: 1978-886X
e - ISSN: 2614-641X

**Table 1. Spesification of The Selected Propeller**

| *No* | *Parameter* | *Value* | *Unit* |
|---|---|---|---|
| 1 | Number of Blade (Z) | 3 | |
| 2 | Propeller Diameter | 4.75 | m |
| 3 | Maximum Diameter (Dmax) | 5.066 | m |
| 4 | Expanded Area Ration (Ae/A0) | 0.534 | |
| 5 | Pitch Ratio (P/D) | 0.7 | |
| 6 | P/Dmax | 0.7 | |
| 7 | Advance Coefficient (J) | 0.385 | |
| 8 | Minimum J Value (Jmin) | 0.362 | |

Computational Fluid Dynamics (CFD) simulations were conducted under open-water conditions using ANSYS Fluent to evaluate the hydrodynamic performance of the selected Wageningen B-series propeller configurations. The incompressible Reynolds-Averaged Navier–Stokes (RANS) equations were solved using the SST k-ω turbulence model, which was selected for its robustness in predicting boundary-layer behavior and adverse pressure gradients commonly encountered on propeller blades.

The computational domain consisted of two cylindrical regions: a rotating domain enclosing the propeller and a stationary outer domain representing the surrounding fluid. The rotating and stationary domains were coupled using a Multiple Reference Frame (MRF) approach. At the inlet boundary, a uniform axial velocity corresponding to the advance velocity (Va) was prescribed, while a static pressure outlet condition with zero-gauge pressure was applied at the outlet. The propeller blades and hub were modeled as no-slip walls, and the outer boundary of the stationary domain was treated as a symmetry condition to minimize blockage effects. Seawater was used as the working fluid with a density of 1025 kg/m3 Pa·s. Pressure–velocity coupling was handled using the simple algorithm, with second-order discretization schemes applied to the momentum and turbulence equations. Convergence was achieved when the residuals of continuity and momentum equations fell below 10-5 and the monitored thrust and torque values varied by less than 0.5% over successive iterations.

The following Figure 1 presents the solid model results of the propeller, comparing configurations with and without Propeller Boss Cap Fins (PBCF). This comparison highlights the geometric and design differences between the two models, illustrating how the PBCF attachment modifies the propeller structure.

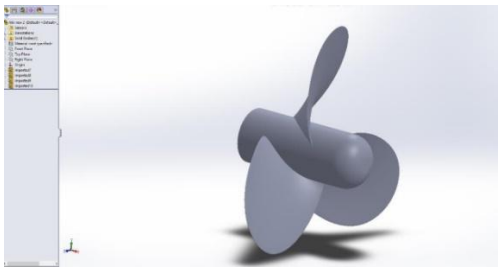

(a)

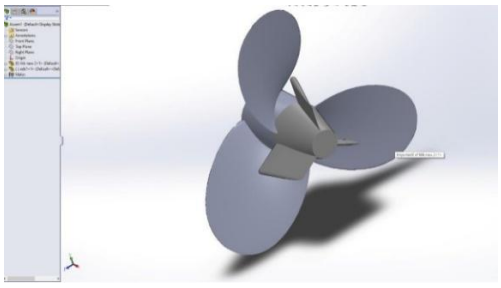

(b)

Figure 2. Solid Model Results of Propeller without PBCF (a) and Propeller with PBCF (b)

The next step is to create the computational domain and set the boundary conditions. In this stage, the main task is to define the size and shape

of the domain. The geometry is edited, typically using SpaceClaim or similar software, to construct the domain around the propeller. For the propeller simulation, the calculation zones are divided into two cylindrical regions: a stationary domain and a rotating domain.

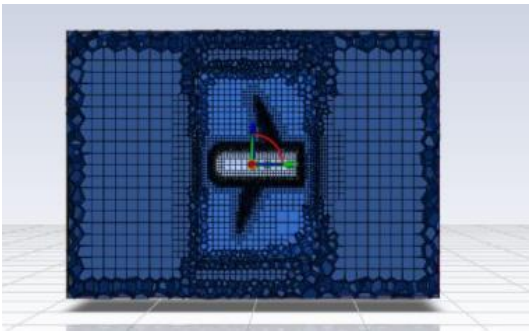

(a)

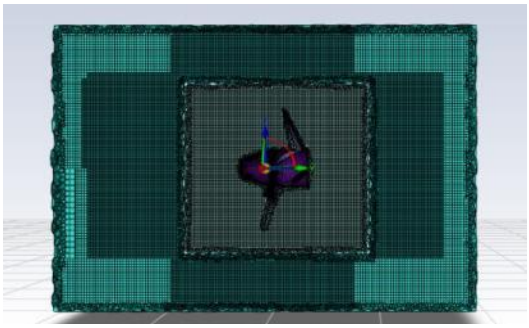

(b)

Figure 3. Steps for Adding Boundary Layers and Generating The Volume Mesh of Propeller without PBCF (a) and Propeller with PBCF (b)

The fluid domain is established, and boundary conditions and material properties are set Ansys. The element size used in this meshing process is m. Simulations compute thrust, torque, efficiency, and other performance metrics under open water conditions. The CFD results are validated against technical limits such as cavitation and material strength.

Once the fluid domain is established, the next step is to generate the mesh as illustrated in Figure 2. This involves first determining the suitable element size to be used for the simulation. Proper mesh sizing is critical to accurately capture the flow characteristics around the propeller while maintaining computational efficiency.

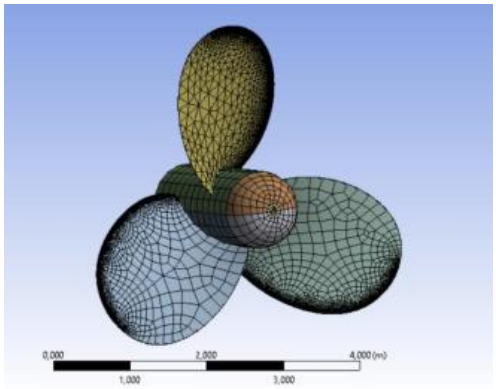

(a)

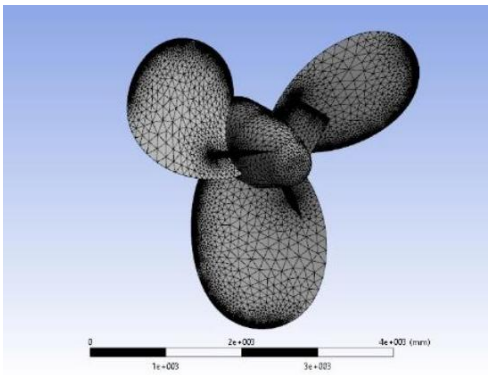

(b)

Figure 4. Meshing Step for Propeller without PBCF (a) and Propeller with PBCF (b)

Unstructured tetrahedral meshes with prism boundary layers are generated. The first-layer thickness is adjusted to maintain $y+ < 2$ across the blade surface. To assess grid independence, five mesh densities were tested, consisting of approximately 1.4, 2.2, 3.0, 4.1, and 5.0 million elements. Grid convergence was evaluated by comparing the resulting thrust coefficient (KT) and torque coefficient (KQ) across these mesh levels. The variation in both KT and KQ between the 3.0 million and 4.1 million element meshes was found to be less than 1.5%, indicating grid-independent behavior. Based on this assessment,

Vol. 19 No. 02, December 2025: page: 107-117
p - ISSN: 1978-886X
e - ISSN: 2614-641X

the mesh with approximately 3.0 million elements was selected for all subsequent simulations as it provides an optimal balance between numerical accuracy and computational cost.

The meshing stage consists of eight steps (1) importing the geometry to input the domain model created in the geometry stage, (2) adding local sizing to specify whether the mesh size around the propeller blades and fins should be smaller, (3) generating the surface mesh, (4) describing the geometry, (5) applying shared topology, (6) updating boundaries, (7) adding boundary layers, and (8) generating the volume mesh. After successfully completing these meshing steps, the model is ready to proceed to the setup stage.

At the setup stage, the meshed and surfaced propeller model undergoes torque and moment analysis using ANSYS Fluent. The fluid flow parameters, including inlet and outlet conditions and boundary constraints within the computational domain, are defined. This solver phase requires input of key parameters such as fluid type, fluid density, advance velocity (Va), and propeller rotational speed (rps). Multiple simulation runs with varying interpolation points are performed to comprehensively assess propeller performance under different operating conditions.

The study employed mesh sizes ranging from 1.4 million to 5 million elements to obtain stable results for thrust and torque parameters. The y+ value at the propeller boundary layer is also critical for mesh validation, ideally maintained below 2 to ensure adequate boundary layer resolution and accurate CFD computations in ANSYS CFX/Fluent. This y+ criterion aligns with best practices for fully resolving the boundary layer on propeller blades, as values below 2 contribute to improved accuracy in capturing pressure distribution and flow separation effects during simulations. Maintaining this range balances computational cost and solution fidelity effectively. Grid independence is considered achieved when the simulation results, such as thrust and torque coefficients, no longer exhibit significant variations with increasing mesh resolution. Typically, three to five mesh densities are tested to evaluate this criterion. In this study, a medium-density mesh comprising approximately 2 to 3 million elements was utilized as the basis for analysis.

From the simulation results, the required data for propeller performance analysis specifically, torque and moment are obtained. These outputs are generated by varying the advance velocity (Va) in the propeller model, enabling comprehensive evaluation of the propeller's behavior across different operational conditions. This step ensures a thorough understanding of how changes in advance velocity affect the resulting torque and moment, which are critical for assessing overall propeller performance in open water scenarios.

CFD results are validated against published Wageningen B-series open-water characteristics for equivalent blade number and geometry. Predicted KT, KQ, and η values show deviations should be within 3–5% of reference experimental data across the tested advance coefficient range. Validated CFD simulations are conducted for propeller configurations with and without Propeller Boss Cap Fins (PBCF). Performance metrics KT, KQ, and η are evaluated over a range of advance coefficients. Comparative analysis is performed to assess how PBCF influences hydrodynamic performance relative to the

optimized baseline propeller.

## RESULTS AND DISCUSSION

### Torque and Thrust Performance

The CFD model (SST k-ω, MRF, $\sim 3 \times 10^6$ cells, $y^+ < 2$) was validated against published Wageningen B-series data with a 3–5 % deviation, and grid-independence gave < 1.5 % change in $K_T$ and $K_Q$ between medium and fine meshes. For all examined advance coefficients, the three-bladed propeller with PBCF shows slightly lower thrust and torque coefficients than the baseline (Table 2 and Table 3). The torque reduction originates from hub-vortex attenuation rather than a loss of propulsive capability.

**Table 2. The Comparison of KT, KQ, J and Propeller Efficiency without PBCF**

| J | $KT_1$ | $10KQ_1$ |
|---|---|---|
| 0.4 | 0.20153 | 0.24851 |
| 0.6 | 0.11419 | 0.17431 |
| 0.8 | 0.03619 | 0.09579 |

**Table 3. The Comparison of KT, KQ, J and Propeller Efficiency with PBCF**

| J | $KT_2$ | $10KQ_2$ |
|---|---|---|
| 0.4 | 0.19943 | 0.23751 |
| 0.6 | 0.10619 | 0.16831 |
| 0.8 | 0.02519 | 0.09479 |

With increasing advance coefficient, both propeller configurations experience a decrease in thrust and torque due to reduced blade loading. However, the relative reduction in torque for the propeller equipped with PBCF remains similar over the investigated operating range. This indicates that the effect of PBCF is mainly governed by local flow phenomena near the hub rather than by overall loading conditions. Such behavior is consistent with previous studies on hub vortex control devices, where torque reduction is commonly associated with weakened rotational flow in the propeller wake rather than with an increase in thrust.

### Efficiency Trends

The open-water efficiency trends for the propellers with and without PBCF are presented in Tables 4 and 5. Open-water efficiency peaks at J=0.6 for the baseline ($\eta = 0.6425$) and at J=0.8 for the PBCF case ($\eta = 0.3513$). The modest efficiency gain at high J is linked to reduced swirl losses when the fins convert hub-induced rotation into axial flow.

**Table 4. The Comparison of KT, KQ, J and Propeller Efficiency without PBCF**

| J | $\eta_{01}$ |
|---|---|
| 0.4 | 0.60820 |
| 0.6 | 0.64250 |
| 0.8 | 0.33931 |

**Table 5. The Comparison of KT, KQ, J and Propeller Efficiency with PBCF**

| J | $\eta_{02}$ |
|---|---|
| 0.4 | 0.56720 |
| 0.6 | 0.60450 |
| 0.8 | 0.35131 |

Vol. 19 No. 02, December 2025: page: 107-117
p - ISSN: 1978-886X
e - ISSN: 2614-641X

Lower peak efficiency of 0.6045 at J = 0.6 indicating that under moderate advance conditions, the fins introduce additional surface area and flow interference that marginally increase viscous losses. However, a notable improvement in efficiency is observed at J = 0.8, where the PBCF configuration achieves an efficiency of 0.3513 compared to 0.3393 for the baseline propeller. Although the absolute difference is modest, this increase is physically meaningful and consistent with the expected operational mechanism of PBCF.

At higher advance coefficients, the hub vortex becomes more pronounced due to reduced blade loading and stronger axial velocity gradients near the hub. The PBCF acts to weaken this vortex by redirecting the swirling flow into a more axial momentum component, thereby reducing rotational losses and improving energy transfer efficiency. This hub vortex suppression mechanism explains why the efficiency benefits of PBCF become more apparent at higher J values rather than near the design point.

The axial-velocity show that the PBCF guides the hub vortex more strongly in the axial direction. As a result, the axial velocity in the near-wake region increases, while the low-pressure area on the suction side near the blade root is reduced. The vorticity magnitude distributions further indicate a decrease in circumferential vorticity, which is in line with the observed reduction in torque. These changes in the flow field explain why the thrust remains nearly constant, whereas the torque and consequently the power consumption decreases.

**Performance Analysis of Propeller with and without PBCF**

The simulation results for the propeller without PBCF reveal that KT, KQ, and efficiency decrease as the advance coefficient (J) increases. The performance metrics are summarized for three specific values of J (0.4, 0.6, and 0.8). Notably, the highest open water efficiency is observed at J = 0.6 with a value of 0.6425, indicating optimal operational efficiency at moderate advance coefficients. Thrust and torque coefficients are both diminished at higher advance coefficients, suggesting reduced load and power requirements under these conditions.

When PBCF is installed, the results present a generally lower KT and KQ across all tested advance coefficients compared to the standard propeller. Specifically, at J = 0.6, efficiency with PBCF is slightly lower (η = 0.6045) than without PBCF, although at J = 0.8, a minor improvement in efficiency with PBCF is exhibited compared to the baseline. These findings are consistent with the literature, where PBCF typically reduces energy loss induced by hub vortices but may yield mixed effects on total hydrodynamic performance depending on the considered operating regime.

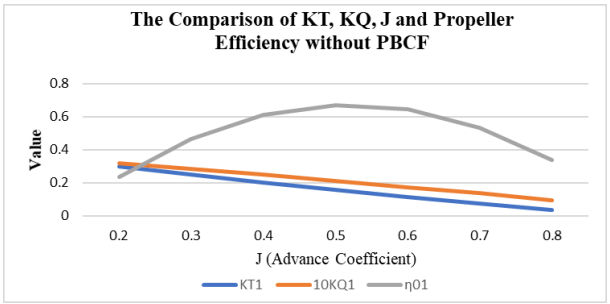


(a)

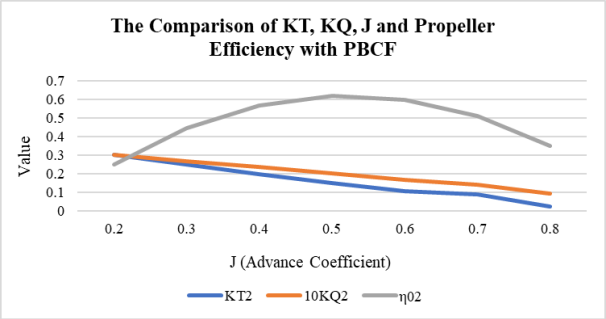


(b)

The torque reduction reflects a weaker swirl in the near-hub wake, which aligns with the lower-pressure-zone suppression described for tip-vortex flows. A weaker swirl produces smoother axial-velocity profiles downstream and diminishes the low-pressure pocket that typically triggers hub-vortex cavitation. At higher J, the efficiency rise can be traced to improved pressure recovery on the suction side of the root region. Flow separation and vortex formation are most likely there; the PBCF-induced reduction in blade-root drag therefore allows a larger fraction of the pressure rise to be converted into useful thrust.

**Uncertainty and Numerical Considerations**

Numerical uncertainty arises from mesh discretisation (< 1.5 % in $K_T/K_Q$), turbulence-model bias, and steady-state assumptions, giving an estimated η uncertainty of ±0.02. Consequently, the small efficiency differences between configurations should be interpreted cautiously, transient CFD or experimental validation would be needed to capture unsteady vortex dynamics and cavitation effects.

**CONCLUSION**

A solver-driven optimization combined with steady-state RANS CFD was applied to the design of Wageningen B-series propellers. The procedure identified a three-blade configuration ($Z = 3$, $D \approx 4.76$ m, $t_{max}/D \approx 0.011$–$0.015$) that satisfies the required thrust of $\approx 4.65 \times 10^5$ N, complies with the 56 MPa material-strength limit, and attains an open-water efficiency of about 51 %. The inclusion of propeller-boss-cap fins (PBCF) modifies the performance envelope. At low to moderate advance coefficients ($J \leq 0.4$) the fins reduce thrust and torque coefficients; however, for higher J values they provide a modest efficiency increase ($\Delta\eta \approx 0.02$) by attenuating the hub-vortex swirl and enhancing pressure recovery near the blade root.

The analysis relies on steady-state RANS, which does not capture unsteady vortex shedding, transient cavitation inception, or detailed blade-root flow separation. The deterministic optimizer explored only a predefined design space, potentially overlooking superior solutions outside the B-series bounds. Mesh discretisation introduces < 1.5 % uncertainty in $K_T/K_Q$, and the turbulence-model selection contributes an estimated efficiency uncertainty of ±0.02.

To support the proposed hub-vortex suppression mechanism, future studies should apply transient CFD or hybrid LES–RANS methods to better capture unsteady hub-vortex behavior and present axial-velocity contours, pressure-coefficient distributions, and vorticity-magnitude plots.

**REFERENCE**

Abar, I.A.C., Utama, I.K.A.P., 2019. Effect of the incline angle of propeller boss cap fins (PBCF) on ship propeller performance. Int. J. Technol. 10, 1056–1064. https://doi.org/10.14716/ijtech.v10i5.2256.

Gaggero, S., 2025. Robust simulation-based

design optimization of marine propellers. Ocean Eng. 321, 120397. https://doi.org/10.1016/J.OCEANENG.2025.120397.

Gypa, I., Jansson, M., Wolff, K., Bensow, R., 2023. Propeller optimization by interactive genetic algorithms and machine learning. Sh. Technol. Res. 70, 56–71. https://doi.org/10.1080/09377255.2021.1973264.

He, N. Van, Cong, N.C., Loi, L.N., 2024. Using Cfd To Investigate the Effect of Ducts on Propeller Performance. J. Nav. Archit. Mar. Eng. 21, 87–101. https://doi.org/10.3329/jname.v21i2.37895.

Mizzi, K., Demirel, Y.K., Banks, C., Turan, O., Kaklis, P., Atlar, M., 2017. Design optimisation of Propeller Boss Cap Fins for enhanced propeller performance. Appl. Ocean Res. 62, 210–222. https://doi.org/10.1016/j.apor.2016.12.006.

Ouyang, W., Zhang, Z., Nie, Y., Liu, B., Vanierschot, M., 2025. Parametric modeling and collaborative optimization of a rim-driven thruster considering propeller-duct interactions. Ocean Eng. 337, 121746. https://doi.org/10.1016/J.OCEANENG.2025.121746.

Ristea, M., Popa, A., Volintiru, O.N., 2025. CFD Design Performance Analysis for a High-Speed Propeller. Appl. Sci. 15. https://doi.org/10.3390/APP15158754.

Sandjaja, I.E., Ariana, I.M., Erwandi, E., Indiaryanto, M., Muryadin, M., Adietya, B.A., 2023. Numerical Analysis of The Effects of Propeller High Thrust Distribution on Propulsion System Performance. Kapal J. Ilmu Pengetah. dan Teknol. Kelaut. 20, 309–319. https://doi.org/10.14710/kapal.v20i3.54715.